Preprint Cambridge Centre for Computational Chemical Engineering ISSN 1473 – 4273

Phase change of polycyclic aromatic hydrocarbon clusters by mass addition

Dongping Chen [1], Tim S. Totton [1], Jethro Akroyd [1], Sebastian Mosbach [1], Markus Kraft [1]

released: 25 July 2013

[1] Department of Chemical Engineering
and Biotechnology
University of Cambridge
New Museums Site
Pembroke Street
Cambridge, CB2 3RA
United Kingdom
E-mail: mk306@cam.ac.uk

Preprint No. 131

Keywords: Sintering, molecular dynamics, coronene, nano-cluster, mechanism, transition

Edited by
Computational Modelling Group
Department of Chemical Engineering and Biotechnology
University of Cambridge
New Museums Site
Pembroke Street
Cambridge CB2 3RA
United Kingdom

Fax: + 44 (0)1223 334796
E-Mail: c4e@cam.ac.uk
World Wide Web: http://como.cheng.cam.ac.uk/

Abstract

We report the first numerical evidence of the phase change of polycyclic aromatic hydrocarbon (PAH) clusters induced by mass addition using molecular dynamics (MD) simulations. We find that an irregular spherical coronene$_{50}$ cluster in the liquid phase is transformed to a columnar particle in the solid phase by coalescing with an identical cluster at 455 K. The evolution of the intermolecular energy and the Lindemann Index are used to monitor the phase change process. The physical reason behind this transformation is the size-dependence of the melting point. We hypothesise that this transformation is a possible mechanism explaining the transition from liquid-phase coalescence to solid-phase fractal growth of soot particles .

Contents

1 Introduction

Soot formation is one of the key environmental problems associated with the operation of practical combustion devices. It is well accepted that mature soot particle appears as aggregates of solid particles even at flame temperatures (i.e. 2000 K) [4]. Following this, models of soot formation often assume that the growth of particles results in completely solid particles [2, 10, 11, 14]. However, several experimental studies have shown this is not the case. Recently, some experimental [20] and numerical [3] evidence suggests that nascent soot particles are liquid-like, especially at sizes smaller than 10 nm. This raises the question about the phase transformation of soot particles from the liquid phase to the solid phase. However, the mechanism by which this phase change takes place is not really understood.

A valid theoretical tool is required to address the dynamics of this phase transformation. Molecular dynamics (MD) is a good candidate as it probes a system at a microscopic level and it has been successfully used in a number studies of the clustering of the soot precursors, i.e. polycyclic aromatic hydrocarbon (PAH) molecules [3, 5, 12, 19]. Specifically, Schuetz and Frenklach [12] first used molecular dynamics to investigate the clustering behaviour of various small PAH molecules. Fiedler et al. [5] investigated the clustering of PAH molecules using a course grain method that allowed MD simulation of 10^6 atoms for hundreds of nanoseconds. This investigation demonstrated the temperature dependence of particle aggregation in flames. More recently, Totton et al. [19] used a novel intermolecular potential rather than the commonly used Lennard-Jones potential to study the dimerisation behaviour of different PAH molecules at various temperatures. The results improved our understanding of the soot inception mechanism. MD simulations have also been used to study melting points of PAH nano-clusters, Chen et al. [3] estimated the melting points of homogenous pyrene and coronene clusters. This work suggested PAH molecules within clusters are highly mobile at flame temperatures and supports the feasibility of sintering of nascent soot particles.

In the present work we use molecular dynamics simulations to monitor the phase change of a coronene$_{50}$ cluster when it coalesces with an identical cluster at different temperatures. We hypothesise that the observed phase change phenomenon plays an important role in the transition of nascent soot particles from liquid phase coalescence (or fully sintered growth) to solid phase fractal growth.

2 Computational method

In our MD simulations, the previously developed isotropic potential (termed isoPAHAP) is used to account for the intermolecular interactions between C–C, C–H and H–H. The details of this potential have been published elsewhere [3, 16–18]. The intramolecular interactions have been determined using the aromatic parameters from the OPLS-AA force field [6] for bonds, angles, dihedrals and improper dihedrals.

Two coronene$_{50}$ clusters were placed next to each other with a distance of 3.5 nm between their centres of mass (COM). Since the spherical diameter of coronene$_{50}$ is 3.5 nm in the

liquid phase [3], this COM distance would result in point contact between the two initial configurations if assuming spherical particles. However, the closest distance between the initial configurations is approximately 0.35 nm due to their irregular surfaces. Calculations were performed for three temperatures, 400 K, 455 K and 500 K. At 400 K, the initial coronene$_{50}$ clusters are in a well-defined solid phase, whilst at 455 K and 500 K, the coronene$_{50}$ clusters are in a liquid phase as suggested by a previous melting study of homogenous coronene clusters [3]. The initial structures were taken from the previous melting work [3]. For the 400 K case, a solid-phase cluster with parallel long stacks originally equilibrated at 400 K is used, whilst for the 455 K and 500 K cases a liquid-like particle with an irregular near-spherical configuration originally equilibrated at 455 K is used (see the initial stages in Figure 1).

We used the same simulation setup as the production runs in previous melting study [3] because the setup was fully tested and successfully mimicked the real systems at the corresponding temperatures. Likewise, the total simulation time is 10 ns for all three cases because the previous work suggests that such a long simulation time will ensure that the resultant configurations reach an equilibrium state. The whole trajectories are examined to identify the evolution of the phase change.

In order to determine when the phase change takes place, we use the methods defined previously [3]: local and global Lindemann Index, intermolecular energy and visual inspection of the morphological change. In each case, the physical quantities (intermolecular energy, Lindemann Index, etc.) were calculated as an average over each 1 ns of the trajectory to identify the state of the system.

The Lindemann Index of an individual molecule within a cluster is expressed as

$$\delta_i = \frac{1}{N-1} \sum_{j \neq i} \frac{\sqrt{\langle r_{ij}^2 \rangle_T - \langle r_{ij} \rangle_T^2}}{\langle r_{ij} \rangle_T}, \tag{1}$$

where N is the number of molecules within the cluster, i and j are the index of ith and jth molecule, respectively, δ_i is Lindemann index of the ith molecule, r_{ij} is the distance between centre of mass of molecule i and that of molecule j, $\langle \dots \rangle_T$ represents an average quantity over 1 ns at temperature T.

The global Lindemann Index δ_{G} of a cluster is expressed as

$$\delta_G = \frac{1}{N} \sum_{i=1}^{N} \delta_i. \tag{2}$$

To explicitly monitor the local phase change phenomenon, the cluster was divided into concentric shells of thickness 3.5 Å, which is the layer separation of a PAH stack [8, 15]. Molecules are assigned to each shell according to the distance to the mass centre of the final configuration. Let S represent a set containing the molecule indices in a particular shell. The local Lindemann Index of each shell is defined as

$$\delta_L = \frac{1}{|S|} \sum_{i \in S} \delta_i, \tag{3}$$

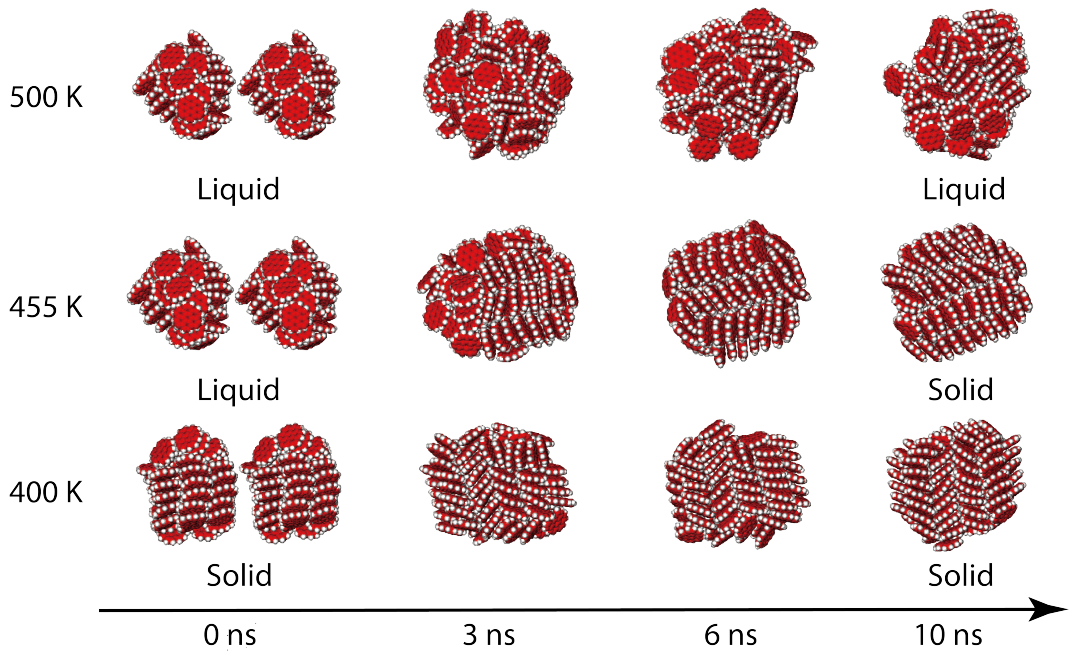

Figure 1: *The morphological evolution of two coronene$_{50}$ clusters coalescing at three temperatures, 400 K, 455 K and 500 K. The white atoms represent hydrogen, the red atoms represent carbon.*

where δ_{L} is local Lindemann Index of each shell and $|S|$ represents the number of molecules in the corresponding shell. Generally speaking, δ_{G} and δ_{L} represent the global and local mobility of the molecules within the investigated clusters respectively.

3 Results

The evolution of the particle morphology was examined visually to monitor the phase changes. In Figure 1, configurations of the resultant particles at four representative stages are shown: 0 ns represents the initial stage, 3 ns represents the stage at which the resultant particle at 455 K starts solidifying, 6 ns represents the stage at which the configurations approach their equilibrated configuration and 10 ns represents the final stage at which all the configurations of the resultant particles have reached their equilibrium states. By viewing the detailed trajectories (attached as supplementary material), the two clusters at 400 K are seen to move towards each other and result in "point contact" within the first 1 ns. In the remaining simulation time, only minor rearrangements of the surface molecules are observed. The final configuration exhibits a certain degree of overlap at the edges of the original clusters. The resultant new cluster maintains a solid-like configuration that is composed of long parallel stacks. At 455 K, the two clusters move towards each other and merge to a greater extent than at 400 K. Subsequent rearrangement results in a transformation from a liquid droplet to a solid particle. Specifically, the morphology was changed significantly from an irregular spherical particle to a columnar particle at approximately 3 ns. At 500 K, the two liquid-like clusters coalesce very quickly, and

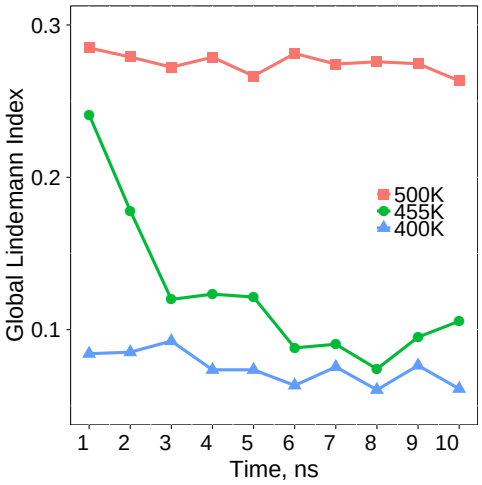

Figure 2: *The global Lindemann Index evolution of two coronene$_{50}$ clusters coalescing at 400 K,455 K and 500 K respectively.*

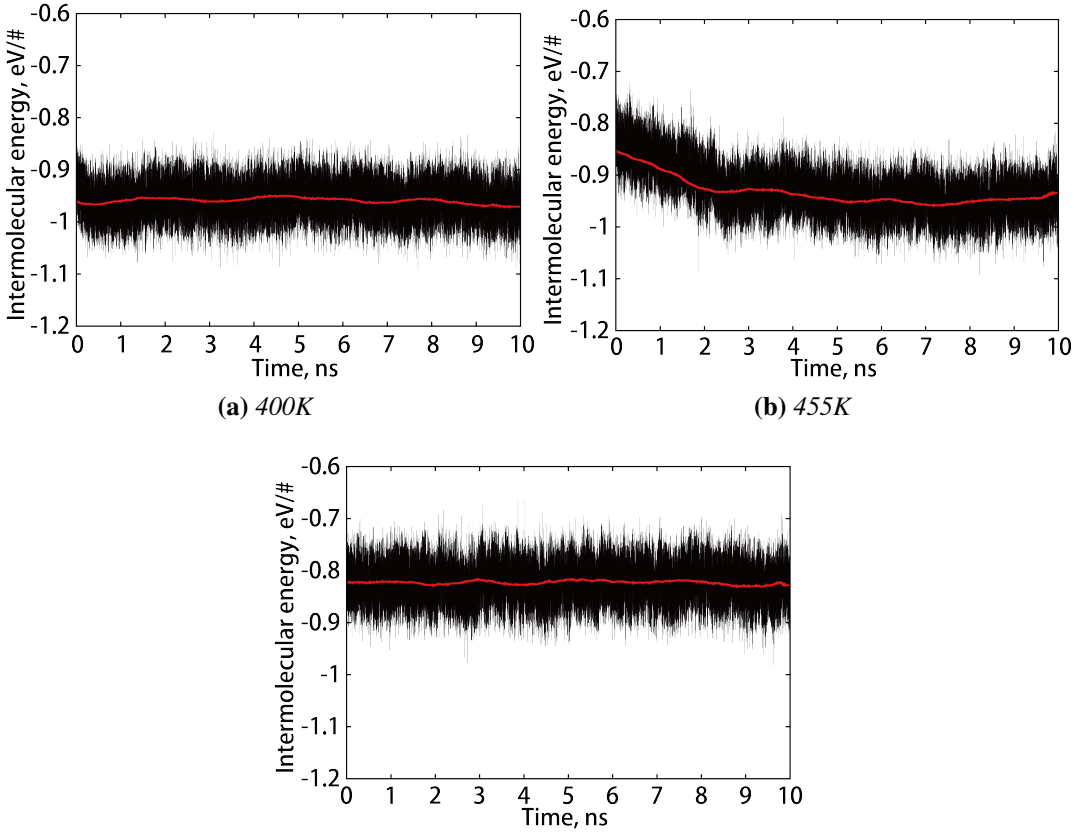

(a) *400K* **(b)** *455K*

(c) *500K*

Figure 3: *The intermolecular energy evolution of two coronene$_{50}$ clusters coalescing at 400 K,455 K and 500 K, respectively. The red lines represent the evolution of the moving average with 1 ns as the window size.*

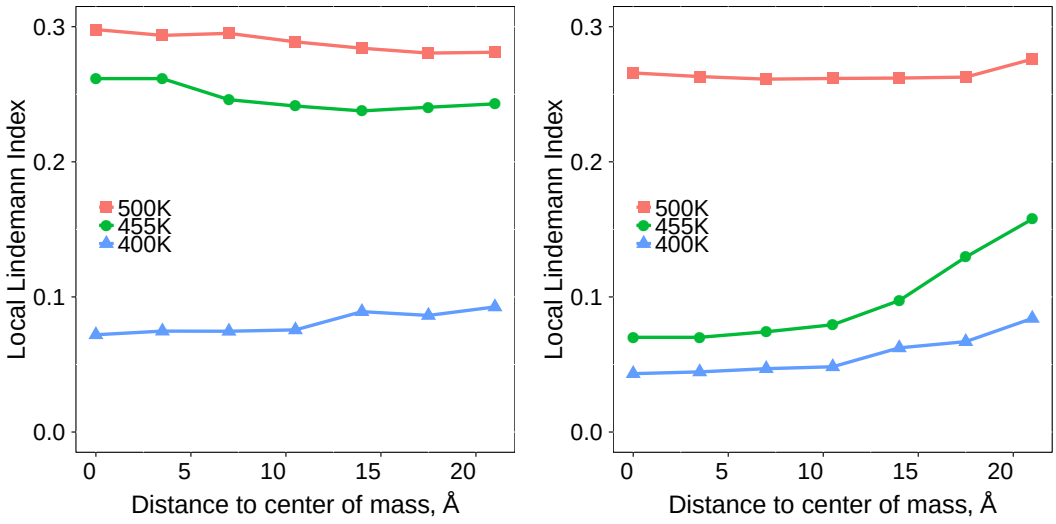

(a) *First 1 ns* **(b)** *Last 1 ns*

Figure 4: *The radial distribution of local Lindemann Index of the merged particles at the early and late stages of coalescence.*

intensive rearrangement is observed across the whole simulation time. The resultant configuration remains liquid-like, as suggested by the melting point. From previous work [3], the resultant coronene$_{100}$ cluster is in a well-defined solid phase at 400 K and 455 K, but in a liquid phase at 500 K. However, at 455 K, the initial coronene$_{50}$ clusters are in the solid phase. Thus, the 455 K case is considered as a transition case due to the size-dependent melting behaviour of coronene clusters [3]. This case allows us to rule out the effect of temperature when observing the phase change after the collision of the two coronene$_{50}$ clusters.

Figure 2 shows that the global mobilities of the molecules within the clusters at 400 K and 500 K are almost constant across the whole simulation time, whilst decrease is seen in the mobility of the molecules in the cluster at 455 K due to the formation of large PAH stacks. This indicates a phase change. Figure 3 further supports the presence of a phase change in terms of the intermolecular energy. At 400 K, the intermolecular energy converged at approximately -0.96 eV per number of molecules in the cluster (or -0.96 eV/#) whilst it was -0.82 eV/# at 500 K. At the transition temperature of 455 K, the intermolecular energy decreased from -0.85 eV/# to -0.94 eV/# during the rearrangements. This shows excellent agreement with the previous study for which a latent energy of 0.084 eV/# was calculated for the coronene$_{100}$ cluster during solidification [3].

To further confirm the phase change phenomenon, we used the local Lindemann Index criterion to identify the phase of the coronene$_{100}$ clusters, at the early and late stages of coalescence. The first 1 ns of the trajectory is interpreted as the early stage of coalescence, while the last 1 ns of the trajectory is interpreted as the late stage. Figure 4a indicates that the 455 K and 500 K cases are in well-defined liquid phases during the early stages of coalescence, as suggested by the high value of local Lindemann Index across the entire clusters, while the 400 K case is in the solid phase as suggested from the reduced value of

the local Lindemann Index. In contrast, Figure 4b indicates that the resultant cluster is in the solid phase by the late stages of coalescence at 455 K as shown by the reduced value of the local Lindemann Index. The curved line can be interpreted as a surface melting phenomenon [3]. It is worth noting that the local Lindemann Indices at 400 K and 500 K show little variation between the early and late stages of coalescence, indicating that no phase change took place. In summary, we observe a phase change in a coronene$_{50}$ cluster at 455 K by coalescing it with an identical cluster. It is shown that this phase change phenomenon only occurs within a transition temperature range, and that no phase change is observed above or below this temperature range.

4 Discussion and Conclusion

The fundamental cause of this phase change phenomenon lies in the nature of the size-dependent melting mechanism [3]. Specifically, the melting point of coronene$_{100}$ is 500 K while that of coronene$_{50}$ is 455 K. Therefore, any form of mass addition due to physical processes, e.g. coalescence with another particle or condensation of molecules from the gas phase, results in an increase in the melting point of the resultant cluster. However, the extent of increase will depend on the amount of mass change. Likewise, mass addition due to chemical processes will also increase the melting point of the resultant cluster due to the fact that the melting point of clusters of larger PAH molecules is higher than that of a corresponding cluster of smaller PAH molecules. Overall, this implies that the mass addition processes can solidify liquid-like particles i.e. change the phase of particles.

When taking a more detailed look at the numerical results, we are able to shed light on the transition from liquid-like growth by particle coalescence to solid-phase fractal growth of soot particles. To understand the details of the coalescence processes performed in the present work, we show the evolution of COM distance between the two initial configurations in Figure 5. This indicates that the coalescence of the two clusters is strongly dependent on temperature. Specifically, the interaction between liquid-like particles always results in coalescence, whilst the interaction between solid particles results in fractal-like growth. At low temperature, i.e. 400 K, the solid particles only exhibit partial overlap and no sign of further merging was found as the COM distance converges to about 1.6 nm, indicating fractal-like growth. At 500 K, the coalescence occurs very quickly (within approximately 2 ns) at which point the COM distance approaches 0 nm and further simulation only causes the rearrangement of the liquid-like configuration. However, at the transition temperature, i.e. 455 K, the COM distance quickly decreases to about 0.7 nm as the liquid-like particles coalesce during the first 3 ns. However, the COM distance subsequently remains constant, indicating that the particle is now in a fractal growth regime and that the resultant cluster has solidified, and no longer display liquid-like behaviour. Thus, the transition temperature case can be considered as a condition that controls the transition from coalescence to fractal growth. The above analysis suggests a mechanism which explains the dynamics of the transition from coalescent growth to solid-phase aggregation in the context of coronene clusters; the transition is caused by phase change due to mass addition. As coronene is a common building block in soot particles, one may apply the above mechanism to improve the understanding of the transition from immediate coales-

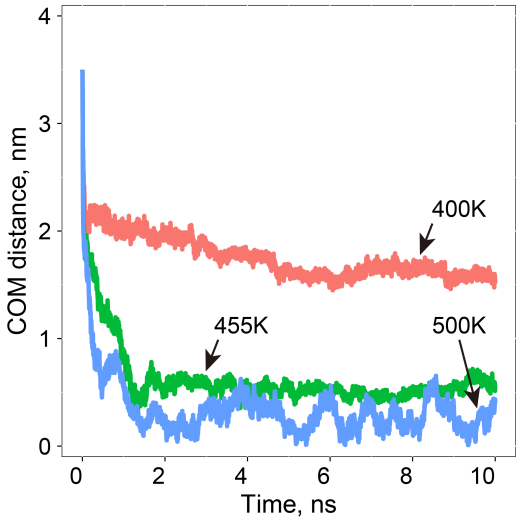

Figure 5: *The evolution of the centre of mass distance between two coronene$_{50}$ clusters at 400 K, 455 K and 500 K, respectively.*

cence to fractal growth of soot particles. While soot generally forms at temperatures much higher than the ones considered here, it should be noted that both the number and size of the molecules involved are much higher as well. For this reason, the mechanism considered here provides a possible explanation for the transition from coalescence to fractal growth even at peak temperatures in a flame. Of course, as the temperature drops in the post-flame region, particles will also solidify. Overall, we note that the above mechanism is not limited to PAH molecules, as size-dependent melting behaviour is commonly observed in other systems, e.g. titanium dioxide [7], silicon [21], nickel [9], iron [13] and gold [1] nanoparticles.

In conclusion, molecular dynamic simulations using a previously developed PAH intermolecular potential were performed to monitor the interactions of two coronene$_{50}$ clusters under various temperatures. Phase changes were identified by monitoring the intermolecular energy and Lindemann Index evolution as well as visual inspection of the morphological evolution of resultant clusters. A clear phase change of the resultant cluster was observed at an intermediate temperature of 455 K, indicating that the phase of an individual particle can be altered by mass addition. The present results can be used to interpret experimental observations of soot particles which suggest that small soot particles are liquid-like while larger soot particles behave as fractal-like solids, even in high-temperature environments.

Acknowledgements

This work was supported by the Singapore National Research Foundation under its Campus for Research Excellence And Technological Enterprise (CREATE) programme. The authors also acknowledge financial support from Shell Research Ltd. and from Churchill College, Cambridge.

References

[1] P. Buffat and J.-P. Borel. Size effect on the melting temperature of gold particles. *Physical Review A*, 13:2287–2298, 1976. doi:10.1103/PhysRevA.13.2287.

[2] D. Chen, Z. Zainuddin, E. Yapp, J. Akroyd, S. Mosbach, and M. Kraft. A fully coupled simulation of PAH and soot growth with a population balance model. *Proceedings of the Combustion Institute*, 34(1):1827 – 1835, 2013. doi:10.1016/j.proci.2012.06.089.

[3] D. Chen, T. Totton, J. Akroyd, S. Mosbach, and M. Kraft. Size-dependent melting of polycyclic aromatic hydrocarbon nano-clusters: A molecular dynamics study. submitted for publication.

[4] R. A. Dobbins. Hydrocarbon nanoparticles formed in flames and diesel engines. *Aerosol Science and Technology*, 41(5):485–496, 2007. doi:10.1080/02786820701225820.

[5] S. L. Fiedler, S. Izvekov, and A. Violi. The effect of temperature on nanoparticle clustering. *Carbon*, 45(9):1786–1794, 2007. doi:10.1016/j.carbon.2007.05.001.

[6] G. A. Kaminski, R. A. Friesner, J. Tirado-Rives, and W. L. Jorgensen. Evaluation and reparametrization of the OPLS-AA force field for proteins via comparison with accurate quantum chemical calculations on peptides. *The Journal of Physical Chemistry B*, 105(28):6474–6487, 2001. doi:10.1021/jp003919d.

[7] V. N. Koparde and P. T. Cummings. Sintering of titanium dioxide nanoparticles: A comparison between molecular dynamics and phenomenological modeling. *Journal of Nanoparticle Research*, 10(7):1169–1182, 2008. doi:10.1007/s11051-007-9342-3.

[8] S. Mosbach, M. S. Celnik, A. Raj, M. Kraft, H. R. Zhang, S. Kubo, and K. Kim. Towards a detailed soot model for internal combustion engines. *Combustion and Flame*, 156(6):1156–1165, 2009. doi:10.1016/j.combustflame.2009.01.003.

[9] E. C. Neyts and A. Bogaerts. Numerical study of the size-dependent melting mechanisms of Nickel nanoclusters. *The Journal of Physical Chemistry C*, 113(7):2771–2776, 2009. doi:10.1021/jp8058992.

[10] A. Raj, M. Sander, V. Janardhanan, and M. Kraft. A study on the coagulation of polycyclic aromatic hydrocarbon clusters to determine their collision efficiency. *Combustion and Flame*, 157(3):523 – 534, 2010. doi:10.1016/j.combustflame.2009.10.003.

[11] M. Sander, R. I. Patterson, A. Braumann, A. Raj, and M. Kraft. Developing the PAH-PP soot particle model using process informatics and uncertainty propagation. *Proceedings of the Combustion Institute*, 33(1):675 – 683, 2011. doi:10.1016/j.proci.2010.06.156.

[12] C. A. Schuetz and M. Frenklach. Nucleation of soot: Molecular dynamics simulations of pyrene dimerization. *Proceedings of the Combustion Institute*, 29(2): 2307–2314, 2002. doi:10.1016/S1540-7489(02)80281-4.

[13] Q. Shu, Y. Yang, Y. T. Zhai, D. Y. Sun, H. J. Xiang, and X. G. Gong. Size-dependent melting behavior of iron nanoparticles by replica exchange molecular dynamics. *Nanoscale*, 4:6307–6311, 2012. doi:10.1039/C2NR30853C.

[14] J. Singh, M. Balthasar, M. Kraft, and W. Wagner. Stochastic modeling of soot particle size and age distributions in laminar premixed flames. *Proceedings of the Combustion Institute*, 30(1):1457 – 1465, 2005. doi:10.1016/j.proci.2004.08.120.

[15] T. S. Totton, D. Chakrabarti, A. J. Misquitta, D. J. Wales, and M. Kraft. Modelling the internal structure of nascent soot particles. *Combustion and Flame*, 157(5):909–914, 2010. doi:10.1016/j.combustflame.2009.11.013.

[16] T. S. Totton, A. J. Misquitta, and M. Kraft. A first principles development of a general anisotropic potential for polycyclic aromatic hydrocarbons. *Journal of Chemical Theory and Computation*, 6(3):683–695, 2010. doi:10.1021/ct9004883.

[17] T. S. Totton, A. J. Misquitta, and M. Kraft. A transferable electrostatic model for intermolecular interactions between polycyclic aromatic hydrocarbons. *Chemical Physics Letters*, 510(1-3):154–160, 2011. doi:10.1016/j.cplett.2011.05.021.

[18] T. S. Totton, A. J. Misquitta, and M. Kraft. Assessing the PAHAP potential with application to the exfoliation energy of graphite. *The Journal of Physical Chemistry A*, 115(46):1368413693, 2011. doi:10.1021/jp208088s.

[19] T. S. Totton, A. J. Misquitta, and M. Kraft. A quantitative study of the clustering of polycyclic aromatic hydrocarbons at high temperatures. *Physical Chemistry Chemical Physics*, 14:4081–4094, 2012. doi:10.1039/C2CP23008A.

[20] H. Wang. Formation of nascent soot and other condensed-phase materials in flames. *Proceedings of the Combustion Institute*, 33(1):41–67, 2011. doi:10.1016/j.proci.2010.09.009.

[21] M. R. Zachariah, M. J. Carrier, and E. Blaisten-Barojas. Properties of silicon nanoparticles: A molecular dynamics study. *The Journal of Physical Chemistry*, 100(36):14856–14864, 1996. doi:10.1021/jp953773w.